J. Fluid Mech. (1992), *vol.* 242, *pp.* 169–192
Printed in Great Britain

Experimental investigation of the field of velocity gradients in turbulent flows

By A. TSINOBER[1], E. KIT[1] AND T. DRACOS[2]

[1] Faculty of Engineering, Tel Aviv University, Tel Aviv 69978, Israel

[2] Institut fur Hydromechanik und Wasserwirtschaft, ETH – Honggerberg, CH-8093 Zurich

(Received 9 March 1990 and in revised form 3 February 1992)

We present results of experiments on a turbulent grid flow and a few results on measurements in the outer region of a boundary layer over a smooth plate. The air flow measurements included three velocity components and their nine gradients. This was done by a twelve-wire hot-wire probe (3 arrays × 4 wires), produced for this purpose using specially made equipment (micromanipulators and some other auxiliary special equipment), calibration unit and calibration procedure. The probe had no common prongs and the calibration procedure was based on constructing a calibration function for each combination of three wires in each array (total 12) as a three-dimensional Chebishev polynomial of fourth order. A variety of checks were made in order to estimate the reliability of the results.

Among the results the most prominent are the experimental confirmation of the strong tendency for alignment between vorticity and the intermediate eigenvector of the rate-of-strain tensor, the positiveness of the total enstrophy-generating term $\omega_i \omega_j s_{ij}$ ($s_{ij} = \frac{1}{2}(\partial u_i/\partial x_j + \partial u_j/\partial x_i)$, $\omega_i = \epsilon_{ijk}\,\partial u_j/\partial x_k$) even for rather short records and the tendency for alignment in the strict sense between vorticity and the vortex stretching vector $W_i = \omega_j s_{ij}$. An emphasis is put on the necessity to measure invariant quantities, i.e. independent of the choice of the system of reference (e.g. $s_{ij} s_{ij}$ and $\omega_i \omega_j s_{ij}$) as the most appropriate to describe physical processes. From the methodological point of view the main result is that the multi-hot-wire technique can be successfully used for measurements of all the nine velocity derivatives in turbulent flows, at least at moderate Reynolds numbers.

1. Introduction

Obtaining experimental information on the field of velocity derivatives in turbulent flows is motivated mostly by the desire to get information on their small-scale structure and dynamics, and in the first place vorticity (for a current review see Foss & Wallace 1989). Other quantities of importance include the rate-of-strain tensor and dissipation (e.g. see Antonia, Shah & Browne 1988 and references therein). In spite of the great number and variety of efforts as described by Foss & Wallace (1989), there are still many doubts as to the reliability of measurement methods of velocity fluctuation derivatives (e.g. Hussain 1986; Aref & Kambe 1988).

For this reason (among others) we have chosen to concentrate our efforts on the grid turbulent flow as the most appropriate for allowing checks of reliability of the measurements, especially of velocity derivatives. The particular significance of this kind of flow follows from the fact that homogeneous (and quasi-isotropic) flow is free from external influences like mean shear, centrifugal forces (rotation), buoyancy, magnetic field, etc. which usually act as organizing factors, favouring the formation

of coherent structures of different kinds (quasi-two-dimensional, helical, etc.). These external influences in many cases can have a strong linear (masking) effect on the intrinsic nonlinear turbulent processes, as in situations described by rapid distortion theory (Hunt & Carruthers 1990). To quote Moffatt (1981, p. 40) '... rapid distortion theory in which nonlinear interactions between turbulent fluctuations are neglected for the duration of the distortion, again illustrates that in some respects shear flow turbulence can be easier than homogeneous turbulence (with zero mean flow)...'. In other words in grid turbulence the nonlinear nature of turbulent flows is manifested more distinctly. We therefore believe that the turbulent grid flow remains one of the most suitable for studying the universal properties of turbulent flows and especially their small-scale structure.

An additional advantage of this flow is that it is more accessible for measurements than, for example, boundary layers, especially in their small-scale structure close to the wall where it is necessary to employ very special microprobes (Willmarth & Sharma 1984; Ligrani, Westphal & Lemos 1989).

Another aspect we would like to stress is the need to measure all the nine velocity derivatives. It is a consequence of the need to obtain invariant quantities (i.e. independent of the system of reference) which are best suited to describing physical processes. Information obtained from measuring quantities which are not invariant in the above sense may appear inadequate, as seen from the three examples below. The first example is one of the results of computations by Rogers & Moin (1987), reported by Narasimha (1990). They clearly demonstrated that the probability density distribution (p.d.d.) of the total dissipation is qualitatively different from that of the square of a single derivative $(\partial u_1/\partial x_1)^2$; while the p.d.d. of the total dissipation is very close to log-normal, which is not the case for the single squared derivative which exhibits a tendency to have a square-root singularity at the origin. The second example is due to Corrsin & Fournier (1982). They showed that the term corresponding to viscous dissipation in the balance equation of turbulent kinetic energy for a single velocity component can have negative regions. This does not contradict the second law of thermodynamics which requires that the total dissipation, i.e. a quantity independent of the choice of the system of reference, has to be positive at each space–time point. The third example is related to the enstrophy generation term $\omega_i \omega_j s_{ij}$ (ω_i are the components of the vorticity vector, s_{ij} is the rate-of-strain tensor) – one of the most important quantities in the dynamics of turbulent flows. It was observed in our recent experiments (Dracos *et al.* 1990) that this term is positive for each record of duration 0.1 s, which for $U = 7$ m/s corresponds to the convection of a 70 cm long strip of fluid past the measuring probe, demonstrating the prevalance of the vortex stretching process. At the same time the term $\omega_1^2(\partial u_1/\partial x_1)$ and similar quantities like $(\partial u_1/\partial x_1)^3$ commonly measured are negative in more than 10% of such records.

This paper is a much fuller version of the parts of Dracos *et al.* (1990) and Tsinober, Kit & Dracos (1991) dealing mostly with the turbulent air flow past a grid. In §2 we describe the experimental facility briefly and the instrumentation in more detail. Section 3 starts with some information on all three components of the velocity field but concentrates on a variety of characteristics of the field of velocity derivatives with the emphasis on invariant quantities like full dissipation, the enstrophy-generation term and fourth-order quantities. Concluding remarks and discussion of the main areas for future improvements are given in §4.

2. Description of experimental procedures and probe performance tests

2.1. *Experimental facility and data acquisition*

The experiments were performed in the open-circuit wind tunnel with a rectangular cross-section 1.4×1.2 m^2, at the Institute for Hydromechanics, ETH, Zurich. The grid was made of wooden rods 1.5 cm in diameter with square mesh of size 6 cm (solidity of 0.44). The free-stream turbulence in the tunnel was about 0.4–0.5%. The measurements were made at distances $x/M = 8$, 17, 30, 38, 64, 90 from the grid and without the grid. Most of the measurements were made at a mean velocity of 7 m/s. Some measurements were also made in the outer region of a turbulent boundary layer at $y/\delta = 0.2$ and 0.8.

The data acquisition was performed by a system based on a MICROVAX computer equipped by an A/D converter (ADF01, DEC) with a throughput frequency rate of 350 kHz and a sample and hold feature. The data sampling rate per channel was 10 kHz. The information sampled at each distance from the grid consisted of 50 separate buffers with 4096 sampling points in every buffer. Spectral characteristics were usually obtained using 200 records with 1024 points in each record. The duration of such a record is ~ 0.1 s, corresponding in most of the experiments to a translation of 70 cm.

2.2. *Twelve-hot-wire probe without common prongs – motivations and development*

We used a multi-hot-wire technique similar to that suggested by Balint (1986), Balint, Vukoslavčević & Wallace (1987, 1988), Balint, Wallace & Vukoslavčević (1991) and Vukoslavčević, Wallace & Balint (1991) which is based on use of arrays consisting of several hot wires (in Balint *et al.* only arrays with three hot wires were used). The voltages obtained from each wire are produced by all three instantaneous components of velocity, which are separated by means of a calibration procedure. This is an intrinsic feature and shortcoming of any method of this kind since any imperfection in the measuring system (mechanical, electronic, etc.) and/or in the experimental facility leading to an error in the signals from the hot wires gives rise to errors in all three velocity components. Therefore these errors can in general be correlated, and consequently, so will many quantities obtained from these velocity components. Errors originating in this way may become dominant when measuring quantities like $\langle u_i u_j \rangle, i \neq j$ (these quantities should vanish in grid turbulence), $u_i \omega_i$, etc.

It is therefore of special importance to make every possible improvement to the measuring system, calibration procedure, etc. So far, we made the following improvements.

One of the possible error sources of the conventional nine-hot-wire probes is the presence of a common prong in every array of three hot wires. This may lead to electronic cross-talking between these hot wires and consequently to unpredictable errors which may significantly contaminate the data. We have checked this point by exciting one wire in an array (with a common prong of common resistance $\leqslant 0.1\ \Omega$, i.e. as in the probe of Balint *et al.*) by a standard pulse signal used for testing the frequency response. The maximum amplitude of the output signal in the two other channels in the same array was about 30% of the output signal of the channel under test instead of being zero as is the case in the new probe without common prongs. Thus, we have developed a multi-hot-wire probe without common prongs. The problem was solved by producing a compound, split prong (instead of the common one), consisting of several (three or four) tungsten wires coated by Teflon and glued

together. It is noteworthy that gluing requires a specially developed Teflon etching procedure. This, along with other reasons, did not allow the conventional sharpening of the tungsten prongs by thermal and mechanical treatment. Instead, an electrochemical erosion method was used, giving a thickness of the tips of the prongs of less than 20 μm. Getting rid of common prongs is also important for reducing the length of individual wires, since with common prongs one has to keep their resistance very large compared to the common resistance, which prevents the scale of the probe being reduced.

We made further special checks of the problems arising from the use of common prongs. We simulated the common prong by connecting the central prongs by a common resistance of 0.1 Ω with the wire resistance of about 9–10 Ω. Among other problems we found that common prongs imposes a serious limit on the overheat ratio, which cannot be raised above 1.3–1.4, thereby increasing the influence of the ambient temperature as compared to higher overheat ratios. This alone shows how serious the problem of cross-talking via common prongs is.

It is specially noteworthy that the inner prongs used instead of the common one were thinner and glued together very close to the tip (~ 2 mm) using microspacers 30 μm thick. Thus this compound prong was ≈ 80 μm only in overall diameter at the tip and in fact was half empty space.

Another problem we encountered is that the single wire (i.e. the one without a partner) is incapable of picking up sufficient information on the corresponding velocity component even in a probe without common prongs. For example consider an array consisting of three slanted wires with two wires in the horizontal plane and the third in the vertical plane in a flow with horizontal mean velocity as, for example, in the grid flow. In this case to the first order all the three wires will sense the component of velocity fluctuations u parallel to the mean velocity; the two horizontal wires will sense the horizontal component of the velocity fluctuations w normal to the mean velocity, and only one vertical wire will sense the vertical component of velocity fluctuations v. Therefore much less information is obtained about the component v as compared to u and w. Indeed, we have observed that the r.m.s. value of v and especially its gradients were systematically lower than those of w (both were smaller than the r.m.s. values of u). The addition of a fourth wire made the probe symmetrical in obtaining information on v and w. In fact, using a four-wire array we had four three-wire arrays. The instantaneous velocity vectors from each of them were used to form a mean, which was adopted as the true value of the instantaneous velocity vector. The results thus obtained were significantly more symmetrical in v and w and their gradients and were independent of rotation of the probe around its axis. We therefore built a probe consisting of twelve hot wires (3 arrays × 4 wires). A schematic of the tip of one array and of the whole twelve-wire probe is shown in figure 1(*a*), while figures 1(*b*) and 1(*c*) show a close-up of an individual array and of a twenty hot-wire probe (i.e. five arrays). The latter was made by adding two arrays to the twelve-wire probe used in the present experiments. The 21st wire is a cold wire (with aspect ratio more than 500) to account for ambient temperature variations and temperature fluctuations up to 1000 Hz. Details on the probe production technology, etc. are given in Tsinober (1988).

Manufacturing the above probe required development of a sophisticated manipulator consisting of three manipulating units each having six degrees of freedom (three translational and three rotational), a special unit for manipulating 2.5 μm wires and a unit for microwelding. Three manipulating units were necessary to manipulate in an independent way the probe, the welding electrode, and the rod

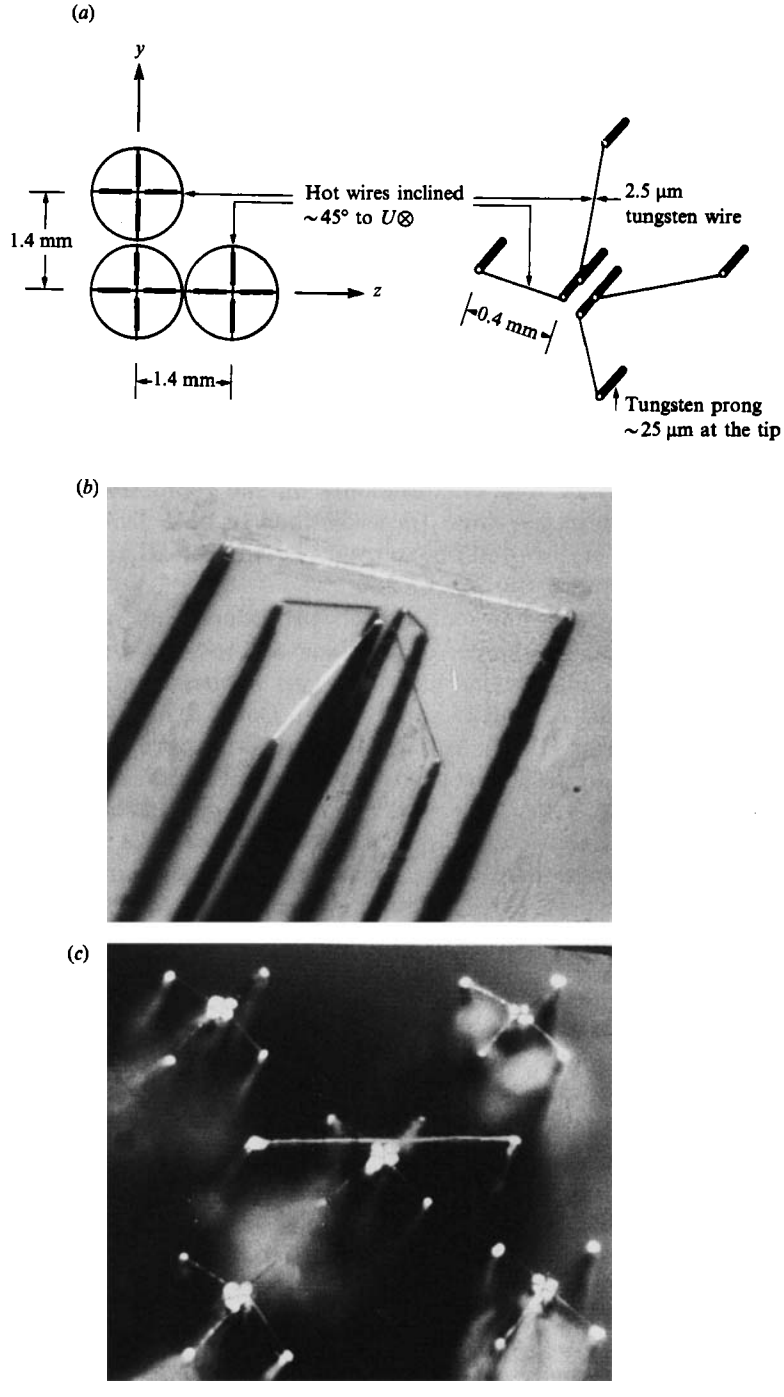

FIGURE 1. (*a*) Schematic of a four-wire array and a twelve-hot-wire probe. (*b*) Close up of an array and (*c*) a 20-hot-wire probe with a cold wire. The twelve-hot-wire probe used in the present experiments consisted of the array in the centre and the two lower arrays in the picture.

carrying a small piece (2–3 mm long) of 2.5 μm wire glued to its tip. The special unit mentioned above in conjunction with one of the manipulating units with six degrees of freedom allowed small pieces of 2.5 μm tungsten wire to be glued at the tip of the steel rods. Note that microwelding the 2.5 μm wires to the 20–25 μm thick tips of the tungsten prongs is quite difficult even when the 2.5 μm wires are platinum plated and the tips of the prongs are nickel plated. Consequently the probe is rather fragile. Recently we improved the technology of the prong tips by tin plating. This makes the welding process much easier and more importantly the probe sturdy enough to be in atmospheric physics applications.

2.3. *Calibration procedure*

The third problem is that the existing calibration procedure (Balint *et al.* 1987, 1988) had the following shortcomings. (i) It employs restrictive assumptions about the symmetry of each array and the flow around the probe as a consequence of using the effective velocity approach for implementation of King's law for multi-hot-wire probes. This results in very high requirements on the geometrical precision of the probe and its alignment in the flow. Imperfections in both lead to uncontrollable errors ('spurious'). (ii) Very limited information, i.e. in vertical and horizontal planes only, is being used to obtain the calibration.

For the above reasons, a new calibration procedure was developed, which is essentially an extension to three dimensions of the least-square polynomial approximation used previously in one and two dimensions by Blackwelder & Haritonidis (1983), Chang & Blackwelder (1990), Oster & Wygnansky (1982), TSI (1978), Wilmarth & Bogar (1977). In the last work an approach based on look-up table was implemented which is essentially the same. Finally, corresponding to our work published in Dracos *et al.* (1990) and Tsinober *et al.* (1991), Dobbeling, Lenze & Leuckel (1990) independently developed a three-dimensional calibration procedure analogous to ours for a four-wire probe similar to that shown in figure 1.

For each combination of three wires in each array (i.e. total $4 \times 3 = 12$) a calibrating function is produced which gives the relation between the three velocity components and the three voltages obtained from each wire in the array. These calibration functions for every velocity component in each array were constructed as three-dimensional polynomials of the fourth order using Chebyshev orthogonal polynomials. Each such calibration function requires determination of 35 coefficients, which were found from 35 equations obtained by a least-square method using the information from measurements at 81 space points (9 yaw and 9 pitch angle positions) and 7 velocities. Owing to the three-dimensional character of the calibration the use of Chebyshev polynomials was essential to reduce the errors and to increase the effectiveness of the determination of the coefficients. The pitch and yaw angles varied within the interval $\pm 12°$.

To produce this amount of information, it was necessary to develop an automatic calibration unit. This consisted of two miniature stepping motors and a mechanical arrangement producing yawing and pitching while the tip of the probe remained in a fixed spatial position. This avoided errors due to flow inhomogeneities. The calibration unit was driven by a controller specially produced for this purpose. One calibration required about 30 min.

The described calibration procedure requires neither very precise alignment of the probe with the mean flow, nor extreme precision of its construction. This was checked by putting the probe at small angles to the mean flow and rotating the probe at various angles (not small) with respect to its axis. The results were essentially the

x/L	8	17	30	38	64	90	B. layer y/δ	
							0.7	0.2
$\langle(\partial u_1/\partial x_1)^2\rangle^{\frac{1}{2}}$	150	64.4	26.5	20.1	15.0	7.95	98.9	114
$\langle(\partial u_1/\partial x_2)^2\rangle^{\frac{1}{2}}$	207	94.4	41.2	31.0	23.8	12.4	150	184
$\langle(\partial u_1/\partial x_3)^2\rangle^{\frac{1}{2}}$	219	99.6	42.6	28.6	24.9	13.2	136	154
$\langle(\partial u_2/\partial x_1)^2\rangle^{\frac{1}{2}}$	175	72.8	32.4	23.7	14.7	9.6	122	139
$\langle(\partial u_2/\partial x_2)^2\rangle^{\frac{1}{2}}$	143	58.0	24.2	19.6	11.1	7.0	106	129
$\langle(\partial u_2/\partial x_3)^2\rangle^{\frac{1}{2}}$	184	79.3	35.2	26.3	16.4	10.8	129	146
$\langle(\partial u_3/\partial x_1)^2\rangle^{\frac{1}{2}}$	175	73.9	32.1	24.5	15.0	9.5	122	144
$\langle(\partial u_3/\partial x_2)^2\rangle^{\frac{1}{2}}$	186	81.4	35.8	27.0	17.7	12.1	136	186
$\langle(\partial u_3/\partial x_3)^2\rangle^{\frac{1}{2}}$	152	66.3	28.9	18.4	13.9	9.1	106	131

TABLE 1. Values of the matrix $\langle(\partial u_i/\partial x_j)^2\rangle^{\frac{1}{2}}$ in s^{-1}

x/L	8	17	30	38	64	90	B. layer y/δ	
							0.7	0.2
$\langle u_1^2\rangle^{\frac{1}{2}}$	52.6	19.7	17.5	14.4	13.7	8.7	80	72
$\langle u_2^2\rangle^{\frac{1}{2}}$	43.8	23.5	14.3	11.7	9.0	7.0	55	38
$\langle u_3^2\rangle^{\frac{1}{2}}$	41.3	23.4	13.8	11.9	8.8	6.7	72	72
$\langle \omega_1^2\rangle^{\frac{1}{2}}$	275	118	52.5	30.6	24.9	16.8	201	252
$\langle \omega_2^2\rangle^{\frac{1}{2}}$	303	134	57.5	40.9	31.1	17.5	196	223
$\langle \omega_3^2\rangle^{\frac{1}{2}}$	292	131	57.0	42.6	30.6	16.9	209	248
$Re_\lambda = u_1\lambda_1/\nu$	96	88	74	67	82	63	415	290

TABLE 2. Values of r.m.s. of velocity fluctuations in $m/s \times 10^2$ and vorticity fluctuations in s^{-1}

same except that they were somewhat better when two wires of each array were located in the plane of pitch and the other two in the plane of yaw.

2.4. *Multi-hot-wire probe performance tests*

The above modifications led to a considerable reduction of errors and improvement of results. For example, the isotropy relations between the terms of the matrix $\langle(\partial u_i/\partial x_j)^2\rangle$ were satisfied within a 15% error (previously 30%, see Kit *et al.* 1987, 1988) as can be seen from table 1 (for isotropy relations between the terms of the matrix $\langle(\partial u_i/\partial x_j)^2\rangle$ see, e.g. Hinze 1975, pp. 188–189). The r.m.s. values of velocity fluctuations are shown in table 2. The incompressibility–Taylor hypothesis test (correlation coefficient C_T between $\partial u_1/\partial x_1 = -U^{-1}\partial u/\partial t$ and $-\partial u_2/\partial x_2 - \partial u_3/\partial x_3$) produced a value of about 0.7 without any smoothing or other similar processing of the raw data, while previously Kit *et al.* (1987, 1988) with a nine-hot-wire probe with common prongs obtained $C_T \sim 0.35$. Balint (1986) reported values of C_T varying from 0.25 to 0.37 which were obtained for various vertical positions of the probe in the boundary layer. Unfortunately the incompressibility–Taylor hypothesis test was never mentioned in the subsequent papers reporting results with nine-hot-wire probe (Balint *et al.* 1987, 1988, 1991; Vukoslavčević *et al.* 1991) in spite of the obvious importance of this check, since it employs the derivatives of velocity fluctuations only and thereby characterizes the reliability of measurements of *instantaneous* velocity gradients.

Note that the checks of the kinematic relations involving velocity derivatives

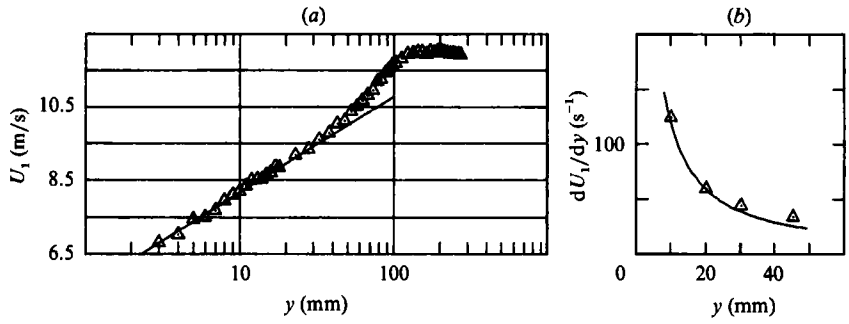

FIGURE 2. (a) Mean velocity profile in a boundary-layer flow, $u^* = 0.47$ m/s, free stream velocity $U_1 = 12$ m/s; (b) Mean velocity gradient: $dU_1/dy = 5.75u^*/y$; △, direct measurement by a multi-hot-wire probe.

given in §3.3.1 can be seen also as characterizing the reliability of measurements of instantaneous velocity gradients. We have also made the simpler check of comparing the mean velocity gradients in several points in a boundary-layer flow deduced from Pitot tube measurements and those obtained directly by the multi-hot-wire probe taking an average of the first-order difference of the instantaneous velocity at two appropriate arrays. The mean velocity profile is shown in figure 2(a) in which the straight line corresponds to a logarithmic profile $U_1/u^* = 5.75\log(y/y_0)$ with $u^* = 0.47$ m/s at free-stream velocity ≈ 12 m/s. The gradient of this velocity $dU_1/dy = 5.75u^*/y$ is shown in figure 2(b) together with the direct measurements of the velocity gradient by the multi-hot-wire probe at four points located in the logarithmic region of the velocity profile. The agreement is very good (the point at $y = 45$ mm is in the region where the velocity profile starts to deviate from the logarithmic one), especially taking into account that the velocity difference at the two arrays was in the range 3–12 cm/s, i.e. only 0.25–1 % of the mean velocity.

We would like to point out that our main aim in presenting some results on the boundary-layer flow is to provide additional support for the proper performance of the probe. They represent only a small part of the available results on the boundary flow, which will be published elsewhere.

Finally, we have made a rather special check on the performance of several four-wire arrays compared to a single-wire probe. This has been done using five-wire probes as shown in figure 1(b). The fifth wire (the long one ~ 1 mm), which was normally used as a cold wire, in this case was operated as a hot wire. It was located ~ 0.15 mm in front of the tip of the multi-hot-wire array and therefore was essentially at the same point. It required a special effort to position this wire just in front of the middle of the tip of the array to avoid thermal interference between the single wire and the four-wire array. Typical results of such a comparison are shown in table 3, which contains the mean velocity U_1, the r.m.s. of the streamwise velocity fluctuations u_1 measured by the four-wire array and by the single wire, and the correlation coefficient $C_{u_1u_1}$ between the two measurements of these fluctuations at three locations from the boundary. One can see that the agreement between the two simultaneous measurements is really very good.

It is noteworthy that the derivatives $\partial u_2/\partial x_2$ and $\partial u_3/\partial x_3$ have been obtained as one sided (figure 1). In our previous paper (Dracos *et al.* 1990) we asserted erroneously that C_T is limited from above by a value less than one independently of how small the probe is. However, assuming isotropy in small scales and approximating the longitudinal correlation function as $f(r) = 1 - ar^2 + br^4$ it can be

	y (mm) = 10 y^+ = 310		y (mm) = 63 y^+ = 1970		y (mm) = 103 y^+ = 3200	
	Array	Wire	Array	Wire	Array	Wire
U_1 (m/s)	7.900	7.834	11.064	11.128	11.875	11.948
u_1 (m/s)	1.046	1.055	0.601	0.627	0.250	0.259
$C_{u_1 u_1}$	0.969		0.987		0.988	

TABLE 3. Comparison of performance of a four-wire array against a conventional single-wire probe at three vertical locations in the boundary layer, $y^+ = yu^*/\nu$. (The position y = 103 mm corresponds to the outer edge of the boundary layer.)

easily shown that within these assumptions $C_T < 1$ for a one-sided approximation of velocity derivatives, while $C_T = 1$ for their central approximation. This shows why it is strongly desirable to use a five-array probe (i.e. twenty hot wires in total) which will enable better evaluation of any other quantities involving velocity derivatives like vorticity, helicity density, enstrophy production term, etc. An additional important benefit from a five-array probe would be that second derivatives of the velocity field could also be evaluated at the same point. The results obtained using such a probe for several flows will be reported elsewhere.

Along with the above-mentioned improvements some shortcomings still remained. The main one is that one-point correlations $\langle u_1 u_2 \rangle / u_1' u_2'$ and $\langle u_1 u_3 \rangle / u_1' u_3'$, where u_i' is the r.m.s. value of u_i, were about 0.1–0.15, i.e. were not as close to zero as they should be in ideally isotropic turbulence (to our knowledge there are no published results on these quantities for grid turbulence). As mentioned above this happens because of intrinsic imperfections of the method leading to errors in u_1, u_2, u_3 which are correlated, as well as because of the imperfections of the flow. Our belief is that these can be reduced further by improving the calibration of the probe, e.g. the mechanical precision of the calibration unit, by using smaller steps in pitch and haw in the vicinity of zero instead of uniform stepping.

Finally, the problem of scale resolution should be specially mentioned. This problem is well known both in laboratory and numerical experiments with the obvious difference that in the first case one has the true flow even when some range of small scales is not resolved. In our experiments the overall probe scale was typically 2–3 times smaller than the Taylor microscale and 4–5 times larger than the Kolmogorov scale, i.e. the scales reasonably resolved were of the order of the Taylor microscale.

Since the velocity gradients on the scale of an individual array at every instant are different from those resolved we did not see any reason to use the latter ones to take into account the former ones as has been done by Balint *et al.* (1986, 1988). Their use of nine equations containing three velocity components and six velocity gradients to resolve the velocities at each array implies the very severe assumption that the velocity gradients across an array are the same as those across the whole probe. This is certainly not true for a flow like our grid flow, since the spatial resolution of the probe is not better than 2.5 mm (its overall size), while the Kolmogorov scale is of the order 0.5 mm. Consequently the gradients due to the eddies in the interval between 0.5 and 2.5 mm are not being taken into account. This in turn can lead to erroneous results. Indeed our own experience in using the calibration procedure developed by Balint (1986), Balint *et al.* (1987, 1988, 1991) and Vukoslavčević *et al.* (1991) was very discouraging. In particular when we used their full set of calibration

equations the deviation from isotropy of velocity derivatives for turbulent grid flow was considerably higher than when the velocity gradients at each array were neglected. Obviously, to overcome this problem the overall scale of the probe should be of the order of the Kolmogorov scale but in this case the velocity gradients at the array scale will be negligible and therefore the calibration procedure will not require to account for them. In any case decreasing the size of individual arrays is essential and will lead to both improvements. With smaller arrays the influence of velocity gradients across them will be reduced and their mutual interference will diminish if the overall scale of the probe is kept the same.

3. Results

3.1. *Velocity fluctuations*

The r.m.s. values of velocity fluctuations exhibit some degree of anisotropy in that the r.m.s. of the longitudinal velocity fluctuations u_1 is about 10–20% higher than that of u_2 and u_3. The r.m.s. values of u_2 and u_3 are equal within $\sim 1\%$. It is noteworthy that all the three arrays produced essentially the same results.

It is also of interest that the same is true of the one-dimensional spectra of u_1, u_2, u_3 which are shown in figure 3. Again, all six spectra of u_2 and u_3 (from the three arrays) are essentially the same, indicating a high degree of isotropy in the plane x_2, x_3; $k_1 = 2\pi fM/U$. The anisotropy of the velocity field is located mostly in the large scales, which is seen from a comparison (see figure 3) of the energy spectrum $E_1(k_1)$ of u_1 calculated from the isotropy relation

$$E_1(k_1) = 2k_1 \int_{k_1}^{\infty} t^{-2} E_2(t)\, \mathrm{d}t,$$

where $E_2(k_1)$ is the energy spectrum of u_2.

It is of interest to look also at the three-dimensional spectrum $E(k)$, computed from the relation

$$E(k) = -\frac{k}{2}\frac{\mathrm{d}E_1(k)}{\mathrm{d}k} - k\frac{\mathrm{d}E_2(k)}{\mathrm{d}k}$$

using an appropriate smoothing procedure for $E_1(k)$ and $E_2(k)$ before taking the first derivatives (see figure 3). A comparison between $k^2E(k)$ and $\Omega(k)$ computed in a similar way to the field of vorticity fluctuations is shown in figure 4 and the agreement between the two is quite reasonable, especially at large k as it should be if isotropy really does exist in the small scales.

As mentioned above, the one-point correlation coefficients $\langle u_1 u_2\rangle/u_1' u_2'$ and $\langle u_1 u_3\rangle/u_1' u_3'$ were about 0.1–0.15, i.e. were not as small as they should be in grid turbulence. In spite of this the triple-correlation behaviour was quite satisfactory. Two of them, $\langle u_1^2(x)\, u_1(x+r)\rangle/u_1'^3$ and $-2\langle u_2^2(x)\, u_1(x+r)\rangle/u_1' u_2'^2$, shown in figure 5, should be equal if isotropy is assumed. It is seen that they are in reasonable agreement with the results for an air grid flow obtained by Frenkiel, Klebanoff & Huang (1979). The fourth moments of all the three velocity components, shown in figure 6, behaved in a quasi-Gaussian manner as did the fourth moment of the streamwise velocity component in Frenkiel *et al.* (1979).

3.2. *Velocity–vorticity relations*

Obviously these relations are among the most difficult to measure since energy is concentrated in much larger scales than the enstrophy. Therefore, the results concerning the tensor $h_{ij} = u_i \omega_j$ should be considered as preliminary and qualitative

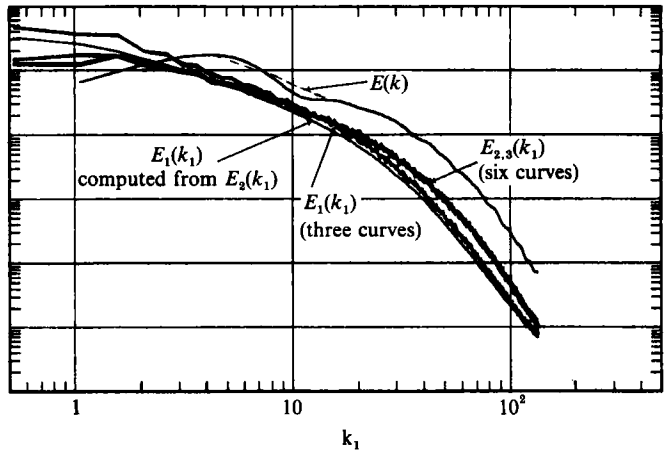

FIGURE 3. Spectra of velocity fluctuations; $x/M = 30$.

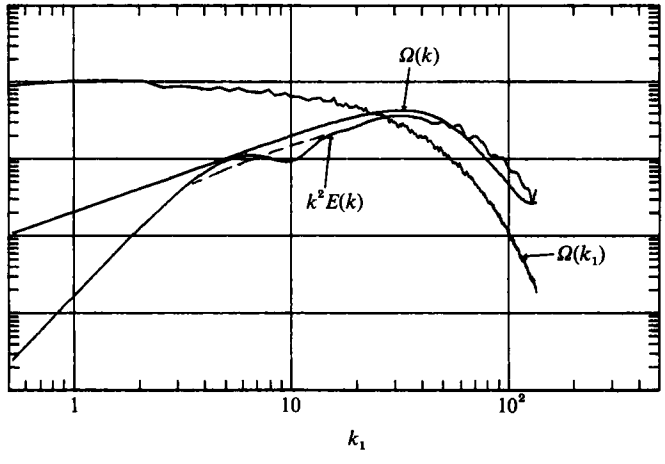

FIGURE 4. Comparison of $k^2E(k)$ and $\Omega(k)$; $x/M = 30$.

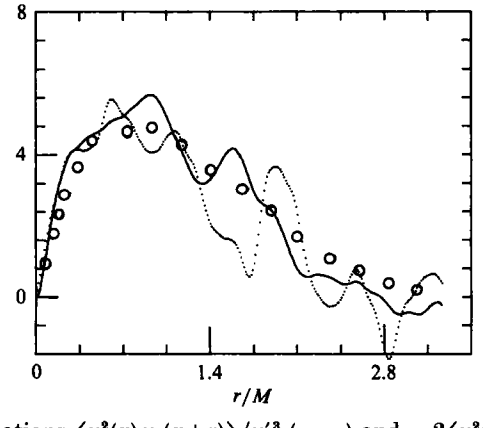

FIGURE 5. Triple correlations $\langle u_1^2(x)\,u_1(x+r)\rangle/u_1'^3$ (——) and $-2\langle u_2^2(x)\,u_1(x+r)\rangle/u_1'\,u_2'^2$(.....), each multiplied by 10^2, where $r = U_{\text{mean}}\,t$; ○, Frenkiel *et al.* (1979).

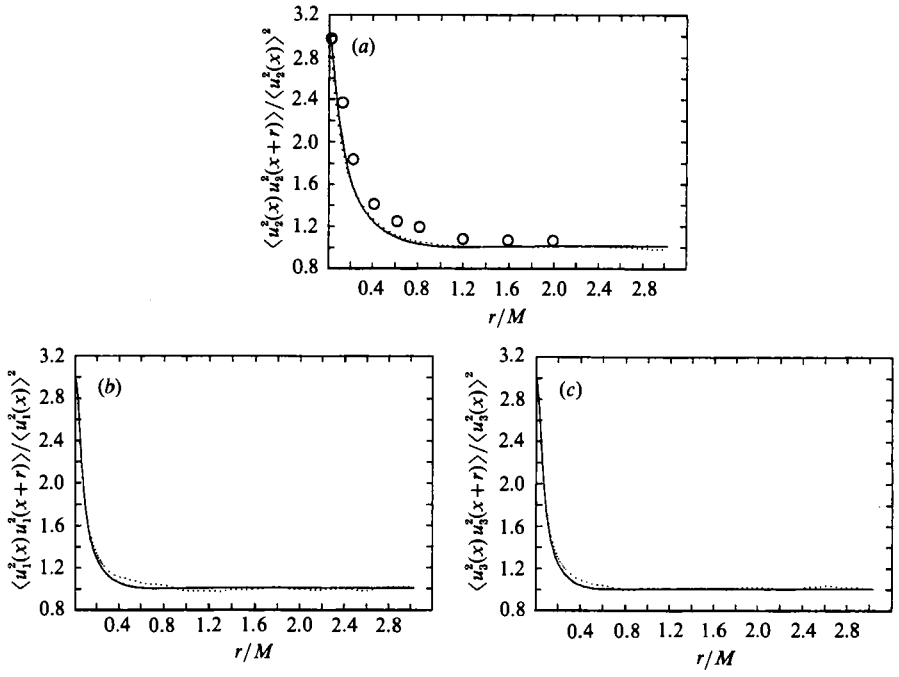

FIGURE 6. Fourth-order correlations for turbulent velocities: ....., measured; ——, Gaussian, ○, Frenkiel *et al.* (1979).

only. The off-diagonal terms of h_{ij} are related to the Lamb vector, and the diagonal ones to helicity.

It is of special interest to look at some properties of the Lamb vector

$$\lambda_k = \epsilon_{ijk} h_{ij} = \epsilon_{ijk} \omega_j u_i \ (\boldsymbol{\lambda} = \boldsymbol{\omega} \times \boldsymbol{u}).$$

Shtilman & Polifke (1989) have found in their direct numerical simulations of decaying box turbulence that the Lamb vector contains a substantial potential part. They calculated the probability density function of the angle between the Fourier image of the Lamb vector and the wave vector $\boldsymbol{k}$ and found that there was a high probability that they were aligned. The implication is that in physical space the Lamb vector should consist mostly of a potential part. A large contribution to this effect may be due to purely kinematic reasons as shown by Tsinober (1990). Experimentally one can have a look at correlations of the type $\langle \lambda_\alpha(x)\lambda_\alpha(x+r)\rangle$, $\alpha = 1,2,3$ and corresponding spectra of λ_α. Simple relations exist between one-dimensional spectra and correlation functions for pure potential vectors assuming isotropy. These are $E_1^{(p)} = -k_1 \mathrm{d}E_{2,3}^{(p)}/\mathrm{d}k_1$ (e.g. see Monin & Yaglom 1975). One-dimensional spectra $E_1^{\lambda}(k_1)$ and $E_{2,3}^{\lambda}(k_1)$ of λ_1 and $\lambda_{2,3}$ respectively are shown in figure 7 together with the curve $\mathrm{E}_{2\,\mathrm{potential}}^{\lambda}$ computed from the $E_1^{\lambda}(k_1)$ using the above relation for a potential vector field. The qualitative indication is that the Lamb vector contains a substantial potential part. This is seen from the comparison of the spectra obtained for the real Lamb vector (figure 7*a*) and those for the Lamb vector obtained as a vector product of two independent vectors (figure 7*b*). These vectors were chosen as velocity and vorticity at large time separation. In the latter case, the spectra for all components are identical in the high-k region, while for the real Lamb vector the spectrum of λ_1 is higher, which corresponds to the tendency of having a

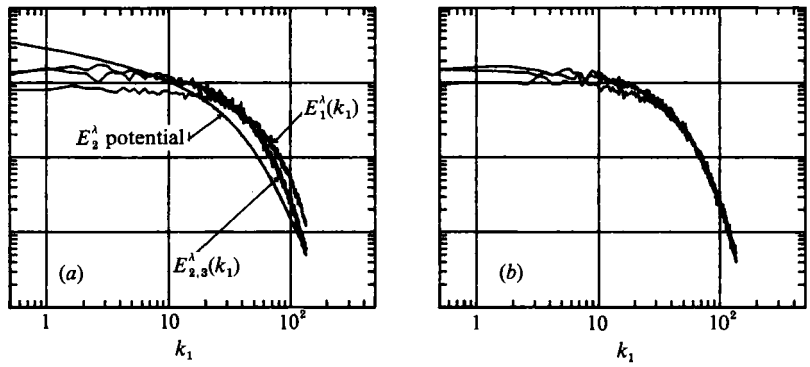

FIGURE 7. (*a*) Spectra of the components of the Lamb vector $\boldsymbol{\lambda} = \boldsymbol{\omega} \times \boldsymbol{u}$. (*b*) As (*a*) but for $\boldsymbol{\omega}$ and $\boldsymbol{u}$ independent; $x/M = 30$.

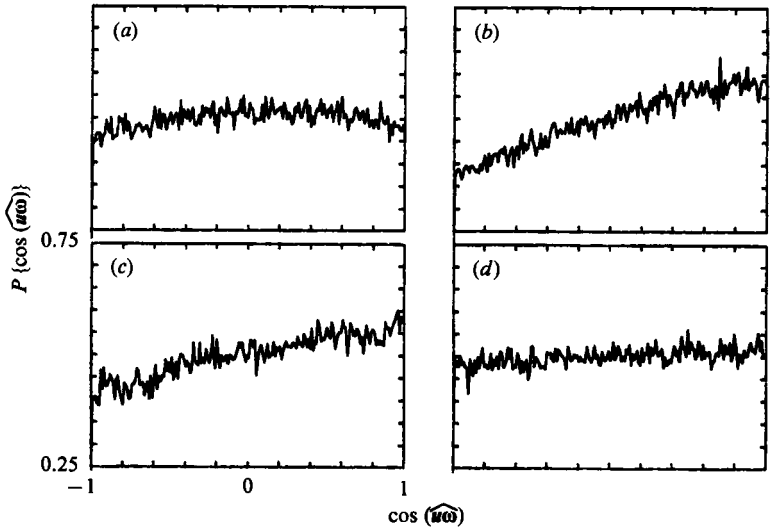

FIGURE 8. Probability density distributions of the cosine of the angle between vorticity and velocity vectors: (*a*) $x/M = 8$; (*b*) $x/M = 17$; (*c*) $x/M = 64$; (*d*) boundary layer: $y/\delta = 0.2$.

substantial potential part. Still, the spectrum $E^\lambda_{2,3,\text{potential}}$ computed from the isotropy relation is different from the real ones, which indicates that the solenoidal part of the Lamb vector is far from negligible.

The alignment between velocity and vorticity (see figure 8) is not as clear as in our previous experiments (Kit *et al.* 1987, 1988; Tsinober *et al.* 1988). However, an important feature is that starting from $X/M = 17$, the probability density function of the cosine between $\boldsymbol{u}$ and $\boldsymbol{\omega}$ becomes asymmetrical, clearly indicating lack of reflectional symmetry in the flow. The quantity $\langle(\boldsymbol{u}\cdot\boldsymbol{\omega})^2\rangle/\langle u^2\rangle\langle\omega^2\rangle = 0.4$ in all the experiments and distances from the grid are as in our previous experiments. Although the mean helicity $\langle h_{ii}\rangle = \langle \boldsymbol{u}\cdot\boldsymbol{\omega}\rangle$ was positive, in almost all experiments its value was within the experimental error.

x/M	8	17	30	38	64	90	B. layer y/δ	
							0.7	0.2
I_1	0.80	0.82	0.85	0.91	0.84	0.84	0.81	0.78
I_2	0.78	0.85	0.91	0.89	0.93	1.06	0.59	0.32

TABLE 4. Values of $I_1 = 2\langle\omega^2\rangle/\langle s_{ij}s_{ij}\rangle$; $I_2 = -\frac{3}{4}\langle\omega_i\omega_i s_{ij}\rangle/\langle s_{ij}s_{jk}s_{ki}\rangle$

x/M	8	17	30	38	64	90	B. layer y/δ	
							0.7	0.2
J_1	7.1	7.3	7.8	7.0	6.6	8.2	7.8	8.6
J_2	7.7	7.2	9.4	7.0	12.0	10.5	6.8	6.8
J_3	6.8	8.8	6.6	7.4	7.7	6.3	6.8	6.5
K_1	8.5	8.8	11.6	11.3	7.8	12.2	7.2	6.7
K_2	12.3	13.8	17.3	11.0	24.0	24.1	10.2	36.0
K_3	10.5	10.9	11.8	22.2	24.5	29.0	4.8	1.00

TABLE 5. Values of $J_\alpha = \langle s_{ij}s_{ij}\rangle/\langle(\partial u_\alpha/\partial x_\alpha)^2\rangle$ and $K_\alpha = -\langle\omega_i\omega_j s_{ij}\rangle/\langle(\partial u_\alpha/\partial x_\alpha)^3\rangle$, $\alpha = 1,2,3$

3.3. *Derivatives of velocity fluctuations*

3.3.1. *Kinematic relations*

Along with calculations of the matrix $\langle(\partial u_i/\partial x_j)^2\rangle$ and the incompressibility–Taylor hypothesis test mentioned above a more delicate test of velocity derivatives measurements was carried out. It is based on the relation imposed by the condition of *homogeneity only* on the one-point triple correlations of the velocity derivatives. This condition was obtained by Townsend (1951) and Betchov (1956) and is as follows:

$$\langle s_{ij}s_{jk}s_{ki}\rangle = -\tfrac{3}{4}\langle\omega_i\omega_j s_{ij}\rangle,$$

where $s_{ij} = \frac{1}{2}(\partial u_i/\partial x_j + \partial u_j/\partial x_i)$ is the rate-of-strain tensor and $\omega_k = \epsilon_{ijk}\partial u_j/\partial x_i$ is the vorticity vector.

The value of the ratio $-\frac{3}{4}\langle\omega_i\omega_j s_{ij}\rangle/\langle s_{ij}s_{jk}s_{ki}\rangle$ obtained from experimental data at different values of x/M is given in table 4. It is seen that the experimental values for the grid flow are quite close to unity, except for the cross-section closest to the grid, while for the boundary layer this ratio is essentially different from unity as can be expected for a non-homogeneous flow.

Many more relations between triple correlations of velocity derivatives are imposed by isotropy (e.g. Townsend 1951; Champagne 1978, p. 106). The one which is generally used relates to the enstrophy generation term with $\langle(\partial u_1/\partial x_1)^3\rangle$:

$$\langle\omega_i\omega_j s_{ij}\rangle = -\tfrac{35}{2}\langle(\partial u_1/\partial x_1)^3\rangle.$$

The values of the ratio $\langle\omega_i\omega_j s_{ij}\rangle/\langle(\partial u_\alpha/\partial x_\alpha)^3\rangle$ (no summation over Greek subscripts 1, 2, 3) are shown in table 5. It is seen that these values are mostly smaller than 17.5 most probably due to insufficient resolution of the small scales.

3.3.2. *Dynamically relevant quantities*

First we show some characteristics of dissipation fluctuations $\eta = \epsilon - \langle\epsilon\rangle$ (table 6): $\langle\eta^2\rangle^{\frac{1}{2}}/\langle\epsilon\rangle$, skewness S_η and flatness F_η. All these quantities are essentially constant in grid flow, i.e. independent of the distance from grid. The same is true for the ratio

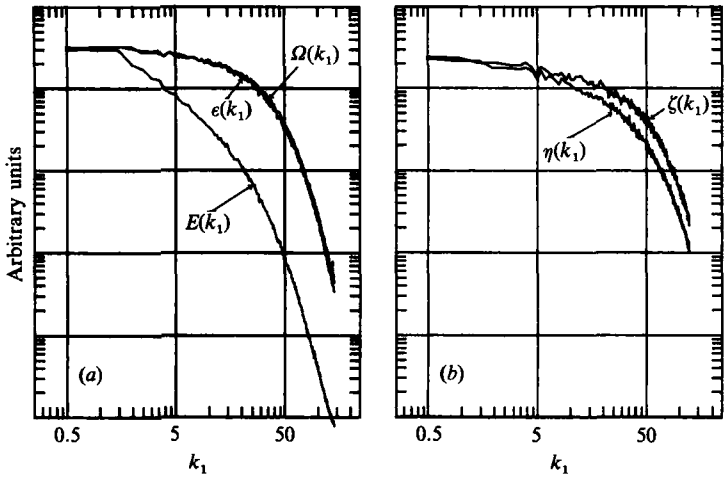

FIGURE 9. One-dimensional spectra of (*a*) energy $E(k_1)$, enstrophy $\Omega(k_1)$ and dissipation $\epsilon(k_1)$, and (*b*) fluctuations of dissipation $\eta(k_1)$ and fluctuations of enstrophy $\zeta(k_1)$; $x/M = 30$.

x/M	8	17	30	38	64	90	B. layer y/δ	
							0.7	0.2
$\langle\eta^2\rangle^{\frac{1}{2}}/\langle\epsilon\rangle$	1.36	1.36	1.37	1.40	1.36	1.36	1.89	3.65
S_η	2.31	2.31	2.40	2.56	2.38	2.29	13.0	106.5
F_η	8.55	8.44	9.36	10.73	9.29	8.06	624	1.97×10^4

TABLE 6. Characteristics of dissipation fluctuations

x/M	8	17	30	38	64	90	B. layer y/δ	
							0.7	0.2
S_1	0.41	0.46	0.50	0.50	0.50	0.50	0.56	0.35
S_2	0.32	0.41	0.44	0.55	0.40	0.37	0.32	0.045
S_3	0.31	0.34	0.38	0.33	0.20	0.14	0.68	−1.61
S	0.12	0.13	0.16	0.16	0.14	0.15	0.16	0.06

TABLE 7. Values of $S_\alpha = -\langle(\partial u_\alpha/\partial x_\alpha)^3\rangle/\langle(\partial u_\alpha/\partial x_\alpha)^2\rangle^{\frac{3}{2}}$ and $S = \langle\omega_i\omega_j s_{ij}\rangle/\langle\omega^2\rangle/\langle(s_{ij}s_{ij}\rangle^{\frac{1}{2}}$

of the spectral densities of ϵ and η (an example of their spectra is shown in figure 9). This seems to be an indication that these quantities are associated with universal properties of the grid flow in small scales. It is noteworthy that the ratio $\langle\eta^2\rangle^{\frac{1}{2}}/\langle\epsilon\rangle$ is a measure of dissipation intermittency (see e.g. Chen *et al.* 1989).

The skewness for the three velocity derivatives are shown in table 7 along with the quantity $\langle\omega_i\omega_j s_{ij}\rangle/\langle\omega^2\rangle\langle s_{ij}s_{ij}\rangle^{\frac{1}{2}}$. It is seen that S_1 agrees well with values known from previous experimental investigations (e.g. Arora & Azad 1980 and references therein). It is also of interest to compare the values of S_1 with those obtained by Herring & Kerr (1982) and Kerr (1985) in numerical simulations of decaying turbulent flow in a box forced at large scales. In the range of Re_λ relevant for our experiments (60–90) they obtained in both simulations that $S_1 = 0.5$. Values of S_2 and S_3 obtained in our experiments are considerably smaller and are in agreement

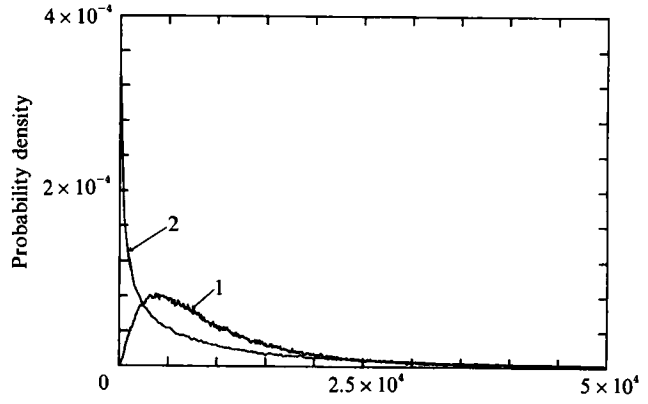

FIGURE 10. Probability density distributions of dissipation (curve 1) and 15 $(\partial u_1/\partial x_1)^2$ (curve 2); $x/M = 30$.

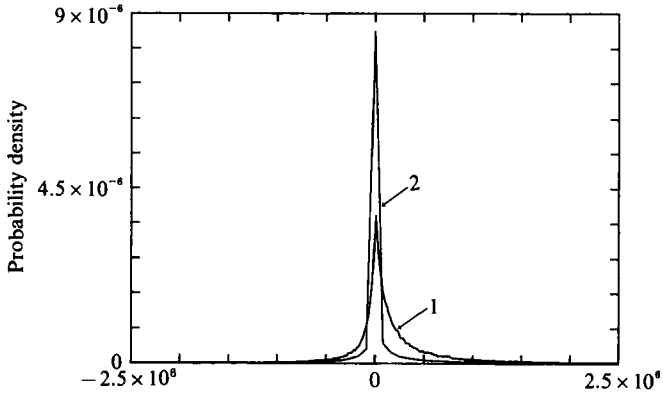

FIGURE 11. Probability density distributions of the enstrophy-generation term $\omega_i \omega_j s_{ij}$ (curve 1), and 17.5 $(\partial u_1/\partial x_1)^3$ (curve 2); $x/M = 30$.

with preliminary measurements in Kit *et al.* (1987), though for isotropic flow S_i should be equal. Our impression is that S_2 and S_3 are smaller than S_1 mainly because of various imperfections of the measuring system. This question requires further investigation.

We would like to emphasize that (see table 7) measurements of the enstrophy-generating term show that its mean is essentially a *positive* quantity. (This was first realized by Taylor 1938.) It was obtained as an average from 200 records each 1024 points long with 10^{-4} s interval between two adjacent points (i.e. 0.1 s record duration or $\approx$70 cm record length). For each such record the enstrophy-generating term was positive. It is noteworthy that the quantity $\langle \omega_1^2 (\partial u_1/\partial x_1) \rangle$ computed for each record was negative for more than 10% of the records. As mentioned in the introduction this points to the importance of measuring quantities that are invariant with respect to our choice of the system of reference, i.e. to measure $\omega_i \omega_j \partial u_i/\partial x_j$. The probability density distribution of ϵ compared with those for $(\partial u_1/\partial x_1)^2$ confirm this point (figure 10) and is in agreement with the computations by Rogers & Moin (1987) (see Narasimha 1990). The same point is clearly also seen from comparing the p.d.d.'s of $\omega_i \omega_j s_{ij}$ and $(\partial u_1/\partial x_1)^3$ (figure 11). Note the asymmetry in the p.d.d. of $\omega_i \omega_j s_{ij}$ – it is larger at positive $\omega_i \omega_j s_{ij}$ which is consistent with the positiveness of the enstrophy-generating term (see also figure 16 and table 5).

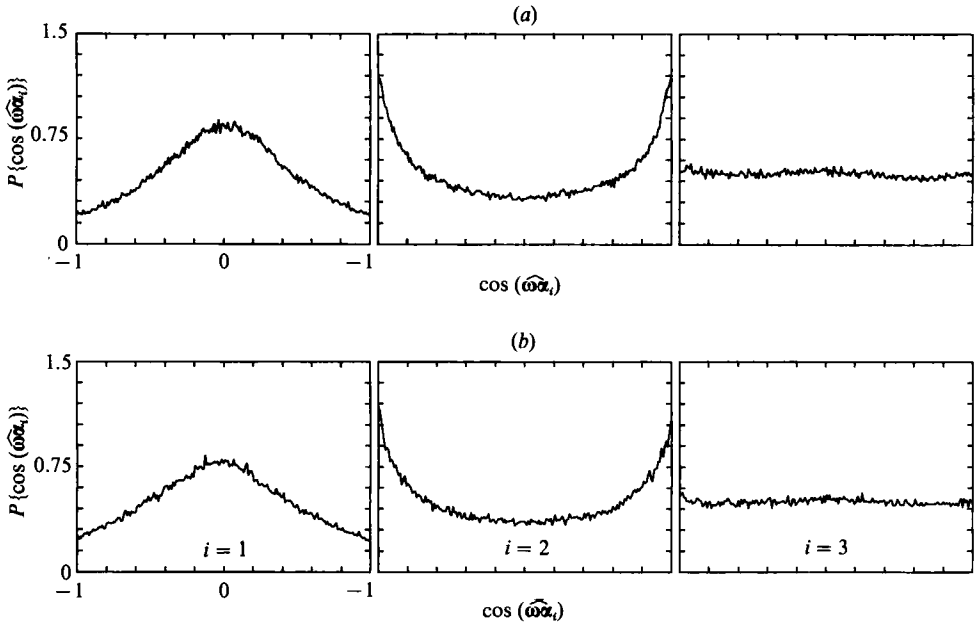

FIGURE 12. Probability density functions of cosine of the angle between vorticity vector and eigenvectors of the rate-of-strain tensor; $\alpha_1 < \alpha_2 < \alpha_3$; $x/M = 30$. (*a*) Grid flow, (*b*) boundary layer, $y/\delta = 0.2$.

x/M	8	17	30	38	64	90	B. layer y/δ		
							0.7	0.2	Gaussian
F_1	3.97	3.99	4.07	4.27	3.95	3.97	9.09	33.8	3
F_2	4.29	4.42	4.48	4.72	4.62	4.46	11.5	46.4	3
F_3	1.04	0.93	0.88	0.88	0.76	0.82	2.09	3.77	1
F_4	4.77	4.90	5.10	5.30	5.21	4.95	12.3	34.9	3

TABLE 8. Fourth-order moments of velocity derivatives

Fourth moments of velocity derivatives defined as

$$F_1 = \frac{15}{7}\frac{\langle s^4\rangle}{\langle s^2\rangle^2}, \quad F_2 = 3\frac{\langle \omega^2 s^2\rangle}{\langle \omega^2\rangle\langle s^2\rangle}, \quad F_3 = 3\frac{\langle \omega_i s_{ij} s_{jk} \omega_k\rangle}{\langle \omega^2\rangle\langle s^2\rangle}, \quad F_4 = \frac{9}{5}\frac{\langle \omega^4\rangle}{\langle \omega^2\rangle^2},$$

where $s^2 = s_{ij}s_{ij}$ are shown in table 8 along with their uncorrelated (i.e. Gaussian) values. The values of F_i are in agreement within 20% with the computational results of Siggia (1981) and Kerr (1985). It is noteworthy that, as in computations by Kerr (1985), in our experiments $F_4 > F_2 > F_1$, i.e. the qualitative tendencies are the same. Also as in their computations, in our experiments F_3 is smaller than 1 implying some alignment in the small-scale turbulent structures. Since F_3 is the normalized variance of the vortex stretching vector $W_i = \omega_i s_{ij}$, $F_3 < 1$ means that there is some reduction of the nonlinear term in the vorticity equation in the sense that $\langle W^2\rangle$ is smaller than its corresponding Gaussian value. This reduction is a small-scale effect different from the reduction of the nonlinearity in the Navier–Stokes equation (Kraichnan & Panda 1989; Shtilman & Polifke 1988; Tsinober 1990; She, Jackson & Orszag 1991).

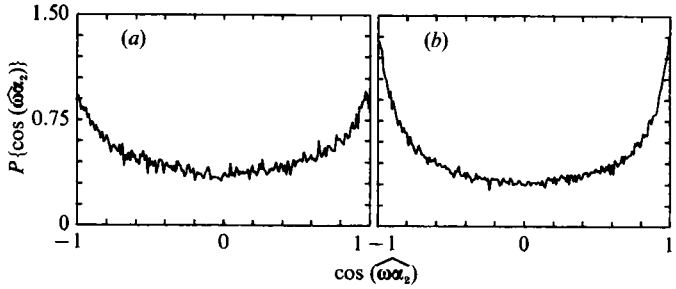

FIGURE 13. Probability density of the cosine of the angle between vorticity and the intermediate eigenvector α_2 for (*a*) $\alpha_2 < 0$; and (*b*) $\alpha_2 > 0$; $x/M = 30$.

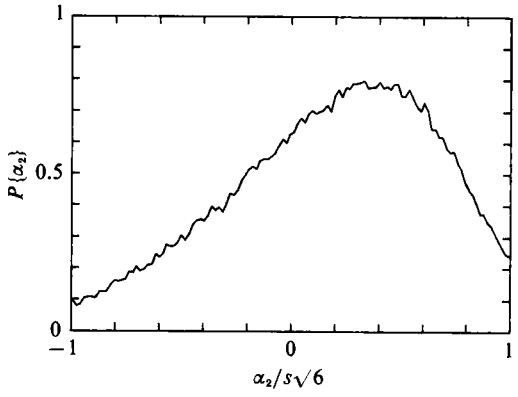

FIGURE 14. Probability density distribution of the intermediate rate of strain α_2; $x/M = 30$.

It is also noteworthy that in our experiments F_1, F_2 and F_4 were about 20% smaller and F_3 about 20% larger than in numerical simulations, i.e. all experimental values of F_i are closer to their Gaussian values, which is consistent with the presence of random noise in the experiments.

3.3.3. *Some local properties*

Among the most basic questions about the properties and dynamics of the vorticity field in turbulent flows are the relations between the vorticity field and the field of the rate-of-strain tensor. Ashurst *et al.* (1987) discovered in their computations quite a peculiar relation between these fields. They found that the vorticity tends to be aligned with the intermediate eigenvector of the rate-of-strain tensor and that the strain in this direction is mostly positive (80%). Our experimental data clearly show the same tendencies (see figure 12), though the alignment is somewhat weaker than in the numerical simulations. Still, the effect is very large, e.g. the maximum to minimum ratio in the p.d.d. of the cosine of the angle between ω and α_2 is more than 4. The alignment between α_2 and ω is considerably stronger for $\alpha_2 > 0$ than for $\alpha_2 < 0$ (see figure 13). This agrees with our observations that in 65% of the sample points the intermediate principal rate of strain was positive in agreement with Betchov's (1956) conclusions and numerical computations by Ashurst *et al.* (1987). This last result is seen better on figure 14 in which the p.d.d. of the normalized intermediate rate of strain $\alpha_2/s\sqrt{6}$ is shown, where $s = (\alpha_1^2+\alpha_2^2+\alpha_3^2)^{\frac{1}{2}}$. Its most probable value is ≈ 0.4. The important point is that the most active part of the

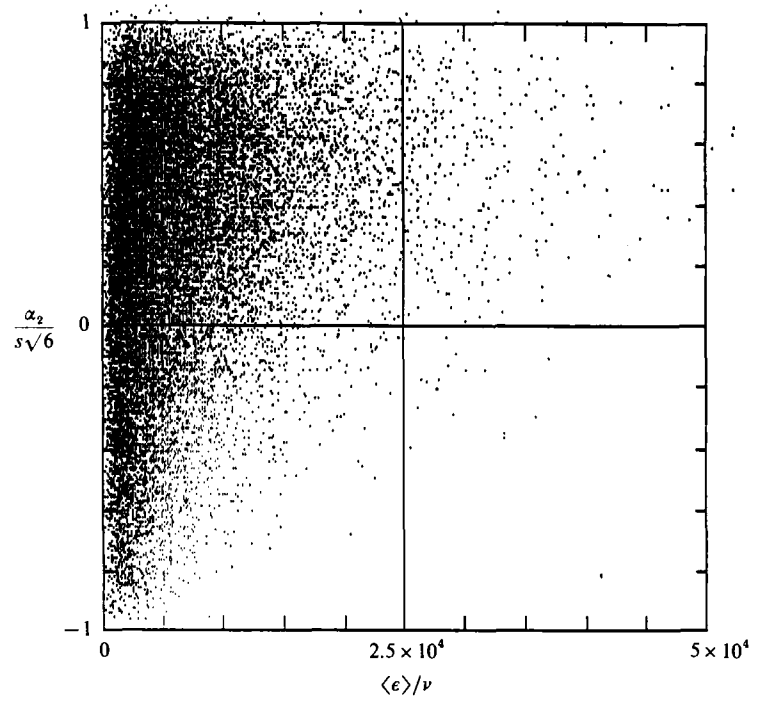

FIGURE 15. Scatter plot of the normalized intermediate rate of strain α_2 versus the energy dissipation; $x/M = 30$.

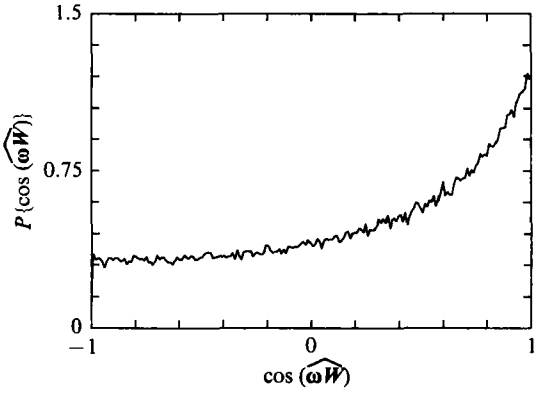

FIGURE 16. Probability density distribution of the cosine of the angle between the vorticity and the vortex stretching vector. $x/M = 30$.

turbulence is located in neighbourhood of this value, which is seen, for example, from the scatter plot of $\alpha_2/s\sqrt{6}$ versus the energy dissipation shown in figure 15. Qualitatively similar behaviour, i.e. maximum activity around $\alpha_2/s\sqrt{6} = 0.4$, is exhibited in scatter plots of $\alpha/s\sqrt{6}$ versus enstrophy and the enstrophy-generation term. Note that the scatter plot shown in figure 15 is very similar to the one obtained by Ashurst *et al.* (1987) (see their figure 1). Also in agreement with their results is the most probable relation between the principal rates of strain, e.g. at $x/M = 30$ this ratio is $-3.8:1:3.1$ while Ashurst *et al.* obtained $-4:1:3$.

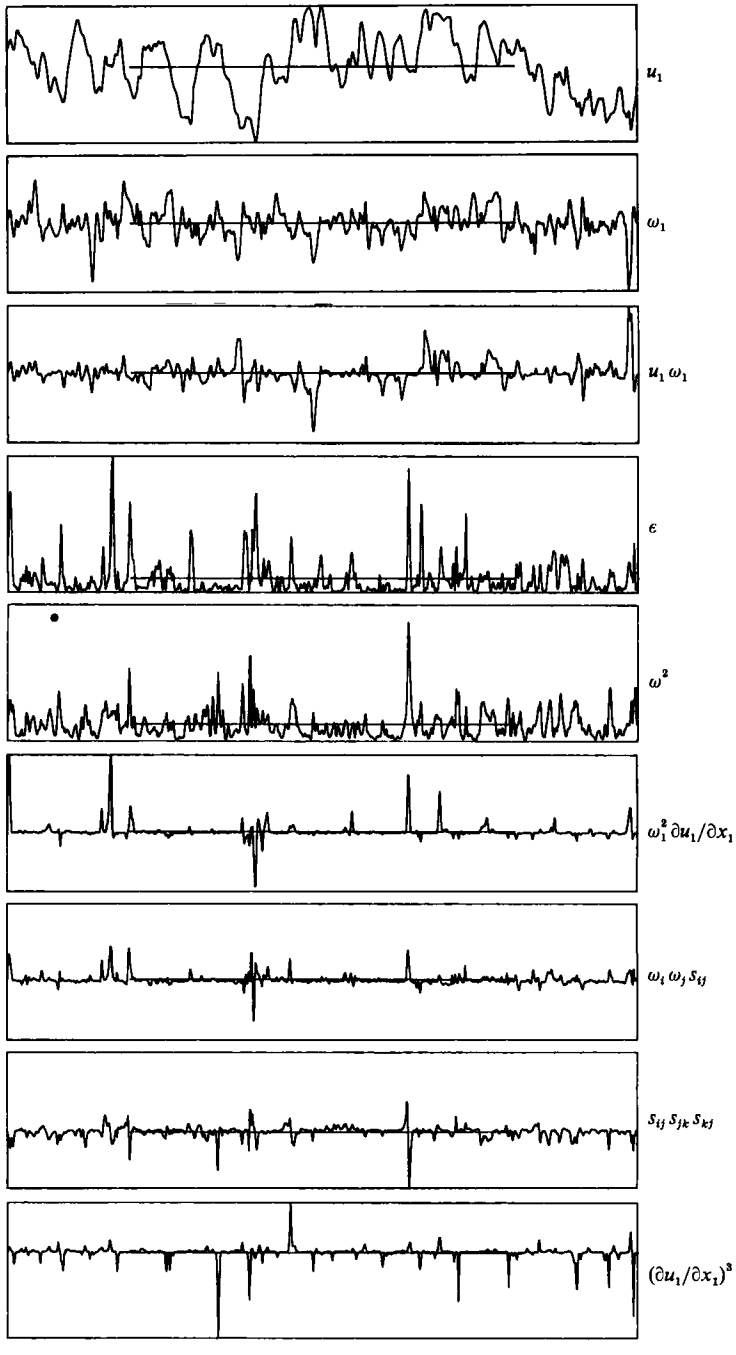

FIGURE 17. Time series of various quantities for one record (70 cm long) in air flow; $x/M = 30$.

Quite reasonable agreement between the experimental results presented here and the numerical ones obtained by Ashurst *et al.* (1987) is a strong indication of the reliability of both, since for such subtle effects it is quite unlikely to be just a coincidence.

We have seen above that the mean of the enstrophy-generating term is essentially

positive (table 6) and moreover it was positive for each record 70 cm long. This is a consequence of the prevalence of the vortex stretching process over the vortex compression. The above irreversible tendency can be characterized locally by considering the p.d.d. of the cosine of the angle between the vorticity vector $\boldsymbol{\omega}$ and the vortex stretching vector $\boldsymbol{W}$ introduced earlier (figure 16). As could be expected this probability density distribution is strongly asymmetrical and is much larger in the region $\theta = 0°$ than in the region $\theta = 180°$. In other words there is a strong tendency for alignment between $\boldsymbol{\omega}$ and $\boldsymbol{W}$ in the strict sense, i.e. a tendency for them to be parallel but not antiparallel. This result along with the positiveness of the enstrophy-generation term are manifestations of the strong non-Gaussianity of the field of velocity derivatives.

Finally in figure 17 we show the time series of various quantities during one record (i.e. 70 cm long). Perhaps the most spectacular is the behaviour of the enstrophy-generating term which exhibit bursts of extremely large amplitude (from 1 to 5 such bursts in one record): quite an intermittency. This amplitude is up to 50 times larger than the average and more than 60% of the contribution to the average of the enstrophy-generating term comes from the fluctuations with amplitude larger than three times the average! The scale of these extremely violent events (or, if one likes, very active structures) is ~ 0.5–1 cm and in between there exist extremely inactive regions (structures). The scale of the latter is an order of magnitude larger than that of the active events. It is noteworthy that the same kind of behaviour is observed in the boundary layer (in its outer part). At this stage we venture to suggest that the enstrophy-generating term, being an invariant (i.e. independent of the system of coordinates and in the Galilean sense), seems to be one of the most appropriate quantities to characterize the structure nature of grid turbulence as well as shear turbulence.

4. Concluding remarks and future work

Our first conclusion is of a technical nature. The results obtained and their comparison with those from direct numerical simulations clearly indicate that multi-hot-wire techniques can be successfully used for measurements of all the nine velocity derivatives in turbulent flows at least at moderate Reynolds numbers. Our belief is that the technique can be considerably improved in two ways: by using a five-array probe; and by the calibration procedure being done not by homogeneous stepping yaw and pitch angles but rather in much denser steps (starting with $\sim 0.25°$) close to zero. Our hope is that this will considerably improve the incompressibility – Taylor hypothesis test and the performance of the system in measuring the off-diagonal terms of the Reynolds stress tensor and the velocity/vorticity tensor. Some improvement of spatial resolution can also be achieved by reducing the scale of the probe. There is no problem in reducing the diameter of each array down to 0.5 mm or even less. We already have experience in producing such an array 0.4 mm in diameter using Platinum – 10% Rhodium wire 1.25 μm in diameter. However, it seems that the requirements for spatial resolution are not as strict as was thought before, at least, for grid turbulence. The reason is that quantities like turbulent dissipation and the enstrophy-generation term scale with the Taylor microscale (cf. Tennekes & Lumley 1974), which is confirmed by our measurements: the Taylor microscales computed according to the conventional definition of λ, from dissipation λ_d and from enstrophy generation λ_e, are all of the same order of magnitude, as is seen from table 9. Note that this is not a circular argument since λ was obtained using

x/M	8	17	30	38	64	90	B. layer y/δ	
							0.7	0.2
λ (mm)	3.5	4.6	6.6	7.3	9.3	11.3	8.2	6.3
λ_d	3.2	4.1	5.6	6.5	7.7	9.0	6.9	5.1
λ_e	4.2	5.1	6.6	7.3	9.4	10.7	9.1	8.5

TABLE 9. Comparison of different Taylor microscales in mm:

$$\lambda^2 = \frac{\langle u_1^2 \rangle}{\langle (\partial u_1/\langle x_1)^2 \rangle}; \quad \lambda_d^2 = \frac{5}{2}\frac{\langle u_i u_i \rangle}{\langle s_{ij} s_{ij} \rangle}; \quad \lambda_e^2 = \frac{(\frac{35}{4})^{\frac{1}{3}}}{3}\frac{\langle u_i u_i \rangle}{\langle \omega_i \omega_j s_{ij} \rangle^{\frac{2}{3}}}.$$

The coefficients for computing λ_d and λ_e were chosen in such a way that the ratios λ_d/λ and λ_e/λ became equal to 1 for isotropic turbulence provided that the skewness $S_1 = -\langle \partial u_1/\partial x_1)^3 / \langle (\partial u_1/\partial x_1)^2 \rangle^{\frac{3}{2}}$ was chosen according to our experimental results to be equal 0.5.

the information from one array only, while λ_d and λ_e were obtained using the information from all three arrays. Thus it is a good indication of proper resolution of these scales. It may therefore happen that the requirements for spatial resolution can be somewhat reduced unless one wishes to evaluate the dissipation of enstrophy, which scales with the Kolmogorov scale. This issue requires further careful exploration especially in view of the results by Wyngaard (1969) and Klewicki & Falco (1990), which claim that for adequate spatial resolution it is necessary that the probe scale should not exceed three Kolmogorov scales. In any case the presently existing technology allows the building of a probe which can be used for applications in atmospheric turbulence. In particular, we intend to perform turbulence measurements at the surface atmospheric layer.

Our second major conclusion is related to the question: does turbulence have a generic, universal structure? We confirmed experimentally the strong tendency for alignment between vorticity and the eigenvector of the intermediate rate-of-strain tensor (discovered numerically by Ashurst *et al.* 1987 for quasi-isotropic and shear turbulence), both for turbulent grid flow and the outer part of the boundary layer. Our opinion is that this property is one of the important universal features of small-scale turbulent flows. Another universal property of three-dimensional turbulent flows is believed to be the prevalence of the vortex-stretching process over the vortex compressing and, closely related to it, the essential positiveness of the enstrophy-generating term. We have demonstrated this to be true via direct measurements of the enstrophy-generation term and the strong tendency for alignment (in the strict sense) between vorticity and vortex stretching vectors. The above results became possible through obtaining quantities like the eigenvectors of the rate-of-strain tensor quantities, which are independent of the system of reference. We have demonstrated the necessity of obtaining other invariant quantities like total dissipation and the enstrophy-generating term. Our suggestion is that quantities of this kind should be among the most appropriate to characterize the structural nature of turbulent flows, e.g. organized motion.

Our main future efforts will be concentrated on improving the technique as mentioned above and its application to turbulent shear flows.

Our special acknowledgement is to Professor J. M. Wallace and Dr J. L. Balint for their kind hospitality during the summer of 1986 and for introducing two of us (A.T.

and E.K.) to all the secrets of their multi-hot-wire technology. This research was supported, in part, by the Eidgenossische Technische Hochschule, Zurich and in part by grant No. 85-00347 from the US–Israeli Binational Scientific Foundation.

REFERENCES

ANTONIA, R. A., SHAH, D. A. & BROWNE, L. W. B. 1988 Dissipation and vorticity spectra in a turbulent wake. *Phys. Fluids* **31**, 1805–1807.

AREF, H. & KAMBE, T. 1988 Report on the IUTAM Symposium: fundamental aspects of vortex motion. *J. Fluid Mech.* **190**, 571–595.

ARORA, S. C. & AZAD, R. S. 1980 Application of the isotropic vorticity theory to an adverse pressure gradient flow. *J. Fluid Mech.* **97**, 385–404.

ASHURST, W. T., KERSTEIN, A. R., KERR, R. A. & GIBSON, C. H. 1987 Alignment of vorticity and scalar gradient with strain rate in simulated Navier–Stokes turbulence. *Phys. Fluids* **30**, 2343–2353.

BALINT, J. L. 1986 Contribution à l'étude de la structure tourbillonnaire d'une couche limité turbulente au moyen d'une sonde a neup fils chauds mesurant le rotationnel. Docteur d'état es sciences, Université Claude Bernard – Lyon, France.

BALINT, J. L., VUKOSLAVČEVIĆ, P. & WALLACE, J. M. 1987 A study of the vortical structure of the turbulent boundary layer. In *Advances in Turbulence* (ed. G. Compte-Bellot & J. Mathieu), pp. 456–464. Springer.

BALINT, J. L., VUKOSLAVČEVIĆ, P. & WALLACE, J. M. 1988 The transport of enstrophy in a turbulent boundary layer. *Proc. Zaric Mem. Inst. Sem. on Wall Turb. Dubrovnik, May 1988.*

BALINT, J. L., WALLACE, J. M. & VUKOSLAVČEVIĆ, P. 1991 The velocity and vorticity vector fields of a turbulent boundary layer. Part 2. Statistical properties. *J. Fluid Mech.* **228**, 53–86.

BETCHOV, R. 1956 An inequality concerning the production of vorticity in isotropic turbulence. *J. Fluid Mech.* **1**, 497–504.

BLACKWELDER, R. F. & HARITONIDIS, J. H. 1983 Scaling of the bursting frequency in turbulent boundary layers. *J. Fluid Mech.* **132**, 87–103.

CHANG, S. I. & BLACKWELDER, R. F. 1990 Modification of large eddies in turbulent boundary layers. *J. Fluid Mech.* **213**, 419–442.

CHAMPAGNE, F. 1978 On the fine-scale structure of the turbulent velocity field. *J. Fluid Mech.* **86**, 67–108.

CHEN, H., HERRING, J. R., KERR, R. M. & KRAICHNAN, R. H. 1989 Non-Gaussian statistics in isotropic turbulence. *Phys. Fluids* A **1**, 1844–1854.

CORRSIN, S. & FOURNIER, J. L. 1982 On viscous dissipation rates of velocity component kinetic energies. *Phys. Fluids* **25**, 583–585.

DOBBELING, K., LENZE, B. & LEUCKEL, W. 1990 Computer-aided calibration and measurements with a quadruple hotwire probe. *Exp. Fluids* **8**, 257–262.

DRACOS, T., KHOLMYANSKY, M., KIT, E. & TSINOBER, A. 1990 Some experimental results on velocity-velocity gradients measurements in turbulent grid flows. In *Topological Fluid Mechanics* (ed. H. K. Moffat & A. Tsinober), pp. 564–584. Cambridge University Press.

FOSS, J. F. & WALLACE, J. M. 1989 The measurement of vorticity in transitional and fully developed turbulent flows. *Advances in Fluid Mechanics Measurements* (ed. M. Gad-el-Hak), Lecture Notes in Engineering, vol. 45. Springer.

FRENKIEL, F. N., KLEBANOFF, P. S. & HUANG, T. T. 1979 Grid turbulence in air and water. *Phys. Fluids* **22**, 1606–1617.

HERRING, J. R. & KERR, R. M. 1982 Comparison of direct numerical simulations with prediction of two-point closures for isotropic turbulence convection a passive scalar. *J. Fluid Mech.* **118**, 205–219.

HINZE, J. O. 1975 *Turbulence.* McGraw Hill.

HUNT, J. C. R. & CARRUTHERS, D. J. 1990 Rapid distortion theory and the 'problems' of turbulence. *J. Fluid Mech.* **212**, 497–532.

HUSSAIN, A. K. M. F. 1986 Coherent structures and turbulence. *J. Fluid Mech.* **173**, 303–356.

KERR, R. M. 1985 Higher order derivatives correlations and the alignment of small scale structures in isotropic numerical turbulence. *J. Fluid Mech.* **153**, 31–58.

KIT, E., TSINOBER, A., BALINT, J. L., WALLACE, J. M. & LEVICH, E. 1987 An experimental study of helicity related properties of a turbulent flow past a grid. *Phys. Fluids* **30**, 3323–3325.

KIT, E., TSINOBER, A., TEITEL, M., BALINT, J. L., WALLACE, J. M. & LEVICH, E. 1988 Vorticity measurements in turbulent grid flows. *Fluid Dyn. Res.* **3**, 289–294.

KLEWICKI, J. C. & FALCO, R. E. 1990 On accurately measuring statistics associated with small scale structure in turbulent boundary layers using hot wire probes. *J. Fluid Mech.* **219**, 119–142.

KRAICHNAN, R. & PANDA, R. 1988 Reduction of nonlinearities in Navier–Stokes equations. *Phys. Fluids* **31**, 2395–2397.

LIGRANI, P. M., WESTPHAL, R. V. & LEMOS, F. R. 1989 Fabrication and testing of subminiature multisensor hot-wire probes. *J. Phys.* E: *Sci. Instrum.* **22**, 262–268.

MOFFATT, H. K. 1981 Some developments in the theory of turbulence. *J. Fluid Mech.* **106**, 27–47.

MONIN, A. S. & YAGLOM, A. M. 1975 *Statistical Fluid Mechanics*, vol. 2, pp. 49–58. MIT Press.

NARASIMHA, R. 1990 Turbulence at the cross roads: the utility and drawbacks of traditional approaches. In *Whither Turbulence? Turbulence at the Crossroads* (ed. J. L. Lumley). Springer. (Available also as a report of Nat. Aeron. Lab. Bangalore, India, 1989.)

OSTER, D. & WYGNANSKI, I. 1982 Forced mixing layer between parallel streams. *J. Fluid Mech.* **123**, 91–130.

ROGERS, M. M. & MOIN, P. 1987 The structure of the vorticity field in homogeneous turbulent flows. *J. Fluid Mech.* **176**, 33–66.

SHE, Z. S., JACKSON, E. & ORSZAG, S. A. 1991 Structure and dynamics of homogeneous turbulence: models and simulations. *Proc. R. Soc. Lond.* A **434**, 101–124.

SHTILMAN, L. & POLIFKE, W. 1989 On the mechanism of the reduction of nonlinearity in the incompressible Navier–Stokes equation. *Phys. Fluids* A **1**, 778–780.

SIGGIA, E. 1981 Numerical study of small-scale intermittency in three-dimensional turbulence. *J. Fluid Mech.* **107**, 375–406.

TAYLOR, G. I. 1938 Production and dissipation of vorticity in a turbulent fluid. *Proc. R. Soc. Lond.* A **164**, 15–23.

TENNEKES, H. & LUMLEY, J. L. 1974 *A First Course in Turbulence*, pp. 87–90. MIT Press.

TOWNSEND, A. H. 1951 On the fine-scale structure of turbulence. *Proc. R. Soc. Lond.* A **208**, 534–542.

TSI 1978 Hot film and hot wire anemometry theory and application. *TSI Tech. Bull.*, TB5.

TSINOBER, A. 1988 Multi-hot-wire probe production for measurements of all nine velocity gradients. *Int. Rep. Fac. Engn. Tel-Aviv University.*

TSINOBER, A. 1990 On one property of Lamb vector in isotropic turbulent flow. *Phys. Fluids* A **2**, 484–486.

TSINOBER, A., KIT, E. & DRACOS, T. 1991 Measuring invariant (frame independent) quantities composed of velocity derivatives in turbulent flows. In *Advances in Turbulence 3* (ed. A. V. Johansson & P. H. Alfredsson), pp. 514–523. Springer.

TSINOBER, A., KIT, E. & TEITEL, M. 1988 Spontaneous symmetry breaking in turbulent grid flow. Presentation at the 17th IUTAM Congress, Grenoble, 21–27 August 1988.

VUKOSLAVČEVIĆ, P., WALLACE, J. M. & BALINT, J. L. 1991 The velocity and vorticity vector fields of a turbulent boundary layer. Part 1. Simultaneous measurement by hot-wire anemometry. *J. Fluid Mech.* **228**, 25–51.

WYNGAARD, J. C. 1969 Spatial resolution of the vorticity meter and other hot wire arrays. *J. Phys.* E: *Sci. Instrum.* **2**, 983–987.

WILMARTH, W. W. & BOGAR, T. 1977 Survey and new measurements of turbulent structure near the wall. *Phys. Fluids* **20**, S9–S21.

WILMARTH, W. W. & SHARMA, L. K. 1984 Study of turbulent structure with hot wires smaller than the viscous length. *J. Fluid Mech.* **142**, 121–149.